

# Colored object recognition by digital holography and a hydrogen Raman shifter

Percival Almoró, Wilson Garcia and Caesar Saloma

National Institute of Physics, University of the Philippines  
Diliman, Quezon City 1101  
[csaloma@nip.upd.edu.ph](mailto:csaloma@nip.upd.edu.ph)

**Abstract:** Multi-wavelength holography is demonstrated with a H<sub>2</sub> Raman shifter that is pumped with an elliptically-polarized pulsed 532 nm beam to produce temporally coherent, intense, polarized output lines. Digital holograms of two-dimensional colored objects are recorded using Raman output lines at 630.4 nm (S<sub>05</sub>, Red), 532 nm (Rayleigh, Green) and 435.7 nm (aS<sub>10</sub>, Blue). Object reconstruction is done numerically via the convolution method and colored object recognition is achieved by multi-channel correlation of the Red, Green, and Blue reconstructions of the reference and the target object.

©2007 Optical Society of America

OCIS codes: (090.0090) Holography; (140.3550) Lasers, Raman; (040.1520) CCD, charged coupled device; (100.0100) Image processing; (100.4550) Optical correlators.

## References and links

1. L. Martínez-León, G. Pedrini, and W. Osten, "Applications of short-coherence digital holography in microscopy," *Appl. Opt.* **44**, 3977-3984 (2005).
2. P. Marquet, B. Rappaz, P. Magistretti, E. Cuche, Y. Emery, T. Colomb, and C. Depeursinge, "Digital holographic microscopy: a noninvasive contrast imaging technique allowing quantitative visualization of living cells with sub-wavelength axial accuracy," *Opt. Lett.* **30**, 468-470 (2005).
3. H. Ye, O. Nilsen, V. Bright, and D. Anderson, "Holographic chemical vapor sensor," *Opt. Lett.* **30**, 1467-1469 (2005).
4. C. Chien, Y. Wu, Y. Chiou, C. Hsieh, Y. Chen, T. Chen, M. Tsai, and C. T. Wang, "Nanoscale deformation measurement by using the hybrid method of gray-level and holographic interferometry," *Opt. Lasers Eng.* **44**, 80-91 (2005).
5. R. McLeod, A. Daiber, M. McDonald, T. Robertson, T. Slagle, S. Sochava, and L. Hesselink, "Microholographic multilayer optical disk data storage," *Appl. Opt.* **44**, 3197-3207 (2005).
6. S. Luo, K. Chen, L. Cao, G. Liu, Q. He, G. Jin, D. Zeng, and Y. Chen, "Photochromic diarylethene for rewritable holographic data storage," *Opt. Express* **13**, 3123-3128 (2005).
7. B. Javidi and E. Tajahuerce, "3D object recognition by use of single-exposure on-axis digital holography," *Opt. Lett.* **30**, 236-238 (2005).
8. D. Kim and B. Javidi, "Distortion-tolerant 3-D object recognition by using single exposure on-axis digital holography," *Opt. Express* **12**, 5539-5548 (2004).
9. H. Bjelkhagen and D. Vukicevic, "Color holography: A technique for the reproduction of paintings," in *Practical Holography XVI and Holographic Materials VIII*, S. A. Benton, S. H. Stevenson, and T. J. Trout, eds., *Proc. SPIE* **4659**, 83-90 (2002).
10. F. Albe, M. Bastide, Y. Lutz, J. Dese, and J. Tribillon, "Color holography: Present State of the research activities at ISL," in *Holography 2000*, T. H. Jeong and W. K. Sobotka, eds., *Proc. SPIE* **4149**, 128-136 (2000).
11. I. Yamaguchi, T. Matsumura, and J. Kato, "Phase-shifting color digital holography," *Opt. Lett.* **27**, 1108-1110 (2002).
12. P. Almoró, M. Cadatal, W. Garcia, and C. Saloma, "Pulsed full-color digital holography using H<sub>2</sub> Raman shifter," *Appl. Opt.* **43**, 2267-2271 (2004).
13. C. Alonzo, W. Garcia, and C. Saloma, "Crosstalk between two-photon and two-color (two-photon) excitation in optical beam induced current generation with two confocal excitation beams," *Opt. Commun.* **270**, 139-144 (2007).
14. D. Diso, M. Perrone, and M. Protopapa, "Rotational Raman scattering dependence on pump polarization," *Appl. Phys. B Lasers and Optics* **70**, 529-536 (2000).
15. Y. Frauel and B. Javidi, "Digital three-dimensional object reconstruction and recognition using integral imaging," in *Three-Dimensional TV, Video, and Display II*, B. Javidi and F. Okano, eds., *Proc. SPIE* **5243**, 140-146 (2003).
16. J. Bermudez, "Object Recognition using cylindrical harmonic filter," *Opt. Express* **12**, 3046-3049 (2004).

17. J. Garcia, J. Valles, and C. Ferreira, "Detection of three-dimensional objects under arbitrary rotations based on range images," *Opt. Exp.* **11**, 3352-3358 (2003).
  18. L. Yaroslavsky, *Digital Holography and Digital Image Processing: Principles, Methods, Algorithms* (Kluwer Academic Publishers, Boston) (2004).
  19. P. Rastogi and A. Sharma, "Systematic approach to image formation in digital holography," *Opt. Eng.* **45**, 1208-1214 (2003).
  20. U. Schnars and W. Juptner, "Digital recording and numerical reconstruction of holograms," *Meas. Sci. Technol.* **13**, R85-R101 (2002).
  21. P. Almero, G. Pedrini and W. Osten, "Complete wavefront reconstruction using sequential intensity measurements of a volume speckle field," *Appl. Opt.* **45**, 8596-8605 (2006).
  22. C. J. R. Sheppard, "Three-dimensional phase imaging with the intensity transport equation," *Appl. Opt.* **41**, 5951-5955 (2002).
  23. P. Hariharan, "Optical systems and light sources," in *Optical Holography* (Cambridge University Press, Cambridge, 1989), 63-77.
- 

## 1. Introduction

Holography has been employed in many applications such as three-dimensional (3D) microscopy [1, 2], interferometry [3, 4], optical data storage [5, 6] and 3D object recognition [7, 8]. Despite its widespread use, the technique still suffers from serious limitations such as lack of color, speckle noise and limited resolution, which could be directly linked to the use of conventional single-wavelength holographic light sources. An attractive alternative is a multi-wavelength light source that can provide all the necessary emission lines for full-color 3D imaging and recognition and variable resolution for interferometric and data storage applications. Multi-wavelength holographic light sources could be assembled from several lasers, either in continuous wave (CW) mode [9] or pulsed mode [10]. They are normally bulky, expensive and require precise timing for synchronized operation. There are single-sources of CW [11] and pulsed [12] multi-wavelength light that are simpler and more compact but the available emission lines in the visible are usually limited to 3 or 4 wavelengths.

The Raman shifter is a multi-wavelength light source with pulsed emission output lines that temporally overlap making it quite suitable for two-color (two-photon) excitation microscopy [13]. The individual emission lines exhibit long temporal coherence lengths and are well-suited for interferometric applications like full-color holography [12]. Generation of additional laser lines in a H<sub>2</sub> Raman shifter has been demonstrated by simply changing the pump polarization [14]. The different vibrational and rotational motions of the H<sub>2</sub> molecules may be accessed with an elliptically polarized pump beam. The relative intensities of the individual lines may also be varied by the beam ellipticity and focusing geometry.

Object recognition by correlation of wavefront intensity or phase is gaining attention due to its potential applications in industry and security. Correlation yields the degree of similarity between two functions. Various techniques and algorithms have been developed for pattern recognition by correlation like integral imaging [15] and mapping of the 3D image using range information [16, 17]. Here, we perform object recognition via digital holography where the complex amplitude of the object wave is reconstructed numerically by Fresnel transform or convolution method [18-20]. We also do colored object recognition by independent correlations of the primary color reconstructions that are rendered scale invariant via the convolution method. Before, object recognition with conventional single-color digital holography was accomplished by correlating the single-channel holographic reconstructions of the reference and target object waves [7, 8]. Holography is carried out with the H<sub>2</sub> Raman shifter and we determine the optical characteristics (wavelengths, polarization, coherence lengths) of the Raman output lines when the shifter is pumped with elliptically polarized light. Our long-term goal is to apply digital holography to 3D spectral imaging for time-resolved analysis of optically-thick samples at high spectral and spatial resolution.

## 2. Reconstruction of digital holograms

Holography starts with the recording of the hologram and the reconstruction of the wave front [18]. During recording, the amplitude and phase of an object wavefront are converted into an intensity distribution by combining the wavefront with a reference beam  $r(x,y)$ . To perform

full wavefront reconstruction, the hologram is illuminated with the conjugate of the reference beam.

As a wavefront reconstruction method, the main advantage of holography is the easy accessibility of the phase information during reconstruction. Other techniques such as the iterative [21] and non-iterative [22] phase retrieval method, require various constraints for approximating the true phase. In digital holography, recording and reconstruction are done with a CCD camera and a computer. Wavefront reconstruction is achieved by multiplying the recorded hologram  $I(x, y)$  with a numerical model of  $r(x, y)$  and by calculating the resulting diffraction field  $U_d(\xi, \eta)$  at the image plane. The field is described by the Fresnel-Kirchhoff diffraction integral [20]:

$$U_d(\xi, \eta) = (1/i\lambda) \iint I(x, y)r(x, y)(1/\rho) \exp(i2\pi\rho/\lambda)dx dy \quad (1)$$

where  $\lambda$  is the illumination wavelength,  $\rho = [d^2 + (x - \xi)^2 + (y - \eta)^2]^{1/2}$  and  $d$  is the reconstruction distance. Under normal incidence of the reference beam,  $r(x, y) \approx 1$ .

### 2.1 Fresnel transform method (paraxial approximation)

When  $d$  is considerably greater than the hologram size, the following paraxial approximation is sufficient [20]:  $U_d(\xi, \eta) \approx \mathcal{F}I(x, y)\exp[(i\pi/\lambda d)(x^2 + y^2)]$  to within a scaling factor, where  $\mathcal{F}$  represents the 2D Fourier transform operation. During CCD recording, the hologram is spatially discretized so that [22]:

$$U_d(r, s) = \mathcal{F}I(k, l)\exp[(i\pi/\lambda d)(k^2\Delta x^2 + l^2\Delta y^2)] \quad (2)$$

where  $\Delta x\Delta y$  is the pixel size in the hologram plane and  $(k, l)$  and  $(r, s)$  are running indices in the hologram and image planes, respectively. The matrix size  $NM$  of  $U_d(r, s)$  is determined by the CCD pixel array.

A drawback of the Fresnel transform method is the unequal pixel sizes of the hologram and image planes that arise from the application of the Fourier transformation. For different reconstruction distances and wavelengths, the reconstruction size also varies by a scaling factor. The pixel size  $\Delta\xi\Delta\eta$  in the image plane is related to that of the hologram plane by:  $\Delta\xi = \lambda d/(N\Delta x)$  and  $\Delta\eta = \lambda d/(M\Delta y)$ . We overcome the scaling problem by treating  $U_d(\xi, \eta)$  as a convolution relation.

### 2.2 Convolution (transfer function) method

The convolution of  $I(x, y)r(x, y)$  with the impulse response  $g(x, y)$  is equal to the inverse Fourier transform of the product of  $\mathcal{F}I(x, y)r(x, y)$  and  $\mathcal{F}g(x, y)$ . For  $r(x, y) \approx 1$ , the diffraction field at a distance  $d$  from the hologram may be expressed as [20]:

$$U_d(r, s) = I(k, l) \otimes g(k, l) = \mathcal{F}^{-1}\{\mathcal{F}I(k, l)\mathcal{F}g(k, l)\} \quad (3)$$

where  $\otimes$  represents the convolution operation, and  $g(k, l) = [(i\lambda)(d^2 + k^2\Delta x^2 + l^2\Delta y^2)^{1/2}]^{-1} \exp\{[(i2\pi/\lambda d)(d^2 + k^2\Delta x^2 + l^2\Delta y^2)^{1/2}]\}$ , is the impulse response under free-space propagation. Because the Fourier transform is applied twice in  $U_d(r, s)$ , the pixel sizes in the hologram and image planes become equal. Hence, the convolution method allows us to achieve image size invariance of the hologram reconstructions even at different illumination wavelengths.

## 3. Multi-channel correlation

Object recognition is accomplished by correlating either the holographic reconstructions  $U(r, s)$  or the holograms  $I(x, y)$  of the reference and target objects. The correlation intensity is given by [7]:

$$C = |\mathcal{F}^{-1}\{\mathcal{F}U_r(r, s)\mathcal{F}U_t(r, s)\}^*|^2 = |\mathcal{F}^{-1}\{\mathcal{F}I_r(x, y)\mathcal{F}I_t(x, y)\}^*|\mathcal{F}g(k, l)|^2|^2 \quad (4)$$

where factors with subscript  $r$  and  $t$  correspond to reference and target objects respectively, and  $[ ]^*$  is the complex conjugate of  $[ ]$ . Correlation peaks indicate the recognition of similar objects. Colored object recognition begins with recording the primary color holograms of the reference and target objects using the  $H_2$  Raman shifter. Separate correlations of the red (R), green (G), and blue (B) reconstructions provide the components of the holographic multi-channel correlator.

#### 4. Experimental setup

Figure 1 shows the experimental setup that includes the Raman shifter and an off-axis digital holographic system. A linearly polarized Q-switched Nd:YAG laser (532 nm, 10 Hz repetition rate, seeded, Spectra Physics GCR-230) produces a 532-nm pump beam that is passed through quarter-wave plate ( $\lambda/4$ ) converting its polarization from linear to elliptical. The elliptically polarized beam is focused into the hydrogen Raman shifter (gas pressure of 0.69 MPa) using lens L1 (focal length: 50 cm). The output of the Raman shifter is collimated using lens L2 (focal length: 50 cm) and then dispersed with a Pellin-Broca (PB) prism. The output of the Raman shifter is collimated using lens L2 (focal length: 50 cm) and then dispersed with a Pellin-Broca (PB) prism.

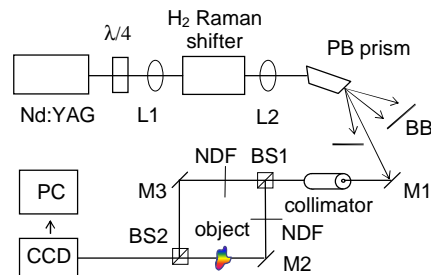


Fig. 1. Experimental setup: Pulsed Nd:YAG laser,  $\lambda/4$  plate, lenses (L1, L2), Raman shifter, Pellin-Broca (PB) prism, beam blocks (BB), mirrors (M1-M3), collimator, beamsplitters (BS1 and BS2), neutral density filters (NDF), test object, CCD camera and computer (PC).

Seventeen Raman output lines were detected at a pressure of 0.69 MPa and 20 mJ excitation energy: a) Vibrational laser line - 435.7 nm ( $AS_{10}$ ); b) Rotational laser lines - 549.1 nm ( $S_{01}$ ), 567.4 nm ( $S_{02}$ ), 587 nm ( $S_{03}$ ), 607 nm ( $S_{04}$ ), 630.4 nm ( $S_{05}$ ), 460.2 nm ( $AS_{05}$ ), 472.9 nm ( $AS_{04}$ ), 486.4 nm ( $AS_{03}$ ), 500.7 nm ( $AS_{02}$ ), 515.9 nm ( $AS_{01}$ ); and c) vibrational-rotational laser lines - 632.3 nm ( $S_{10}$ - $AS_{02}$ ), 377.1 nm ( $AS_{20}$ - $S_{01}$ ), 414.5 nm ( $AS_{10}$ - $AS_{02}$ ), 424.8 nm ( $AS_{10}$ - $AS_{01}$ ), 447.1 nm ( $AS_{10}$ - $S_{01}$ ), 459.2 nm ( $AS_{10}$ - $S_{02}$ ).

We have found that the pulse energies of most of the Raman lines are sufficient for off-axis holography. Unwanted reductions in the fringe visibility caused by unwanted polarization changes in the light scattered from the sample [23], are minimized when the reference beam is elliptically polarized. The coherence lengths of the pertinent Raman lines were measured using Michelson interferometry. Coherence length is the path length difference between the reference and probe beams that decreases the fringe contrast of the interference pattern by 37% of the maximum that is obtained at zero path difference. We measured coherence lengths ranging from 0.5 m to 1 m. Also in the setup are beam-conditioning optics, a CCD camera and a computer for the recording and reconstruction of off-axis digital holograms. For our experiments, we utilized the 630.4 nm ( $S_{05}$ , R), 532 nm (Rayleigh, G) and 435.7 nm ( $AS_{10}$ , B) Raman lines. A collimator is used to achieve uniform spatial beam distribution and to maintain the same illumination direction for the RGB beams.

#### 4. Color object recognition

Figure 2 shows the (a) reference and (b) target colored objects in the experiments. They were made from photographic acetates with color films attached. The symbols “NIP” and “U.P.” are of the same font size. The colored objects were positioned 8 cm from the CCD camera (Sony Monochrome XC-75, 480 x 640 pixels) and were illuminated successively by the R, G, and B Raman lines. The holograms were digitized with an 8-bit frame grabber. Before applying the convolution method, the off-axis holograms were spatially-filtered to address the twin-image problem.

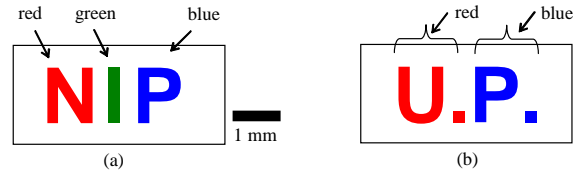


Fig. 2. Colored test objects: (a) Reference and (b) Target. Object dimensions (mm): 1.5 x 3.5 x 0.3.

Figures 3(a)-3(c) and 3(d)-3(e) present the RGB reconstruction channels for the reference (first row) and target (second row) objects, respectively. Color information is recovered using a light source of the required RGB wavelengths. In the green channel [Fig. 3(b) and 3(e)], traces of the red and blue aspects of the objects could still be found due to the broad transmittance of our color filters. The reconstruction channels for the reference and target object were maintained at the same image size even for different wavelength channels via the convolution method.

Also plotted in Fig 3 are the autocorrelations of the (g) R, (h) G, and (i) B reconstructions of the reference object. The cross-correlations of the (j) R, (k) G and (l) B channels of the reference and target objects are also presented. The B channel [Fig. 3(l)] produces the highest and sharpest correlation peak ( $C_{\max} = 0.72$ ) because the blue-colored aspects (letter ‘P’) in the reference and target objects are quite similar. The green channel [Fig. 3(k)] on the other hand, yields the lowest correlation value since the target object does not contain any green colored aspect. The results in Fig. 3 reveal that accurate recognition has been achieved for objects of similar colors and shapes with a Raman shifter and multi-channel correlation.

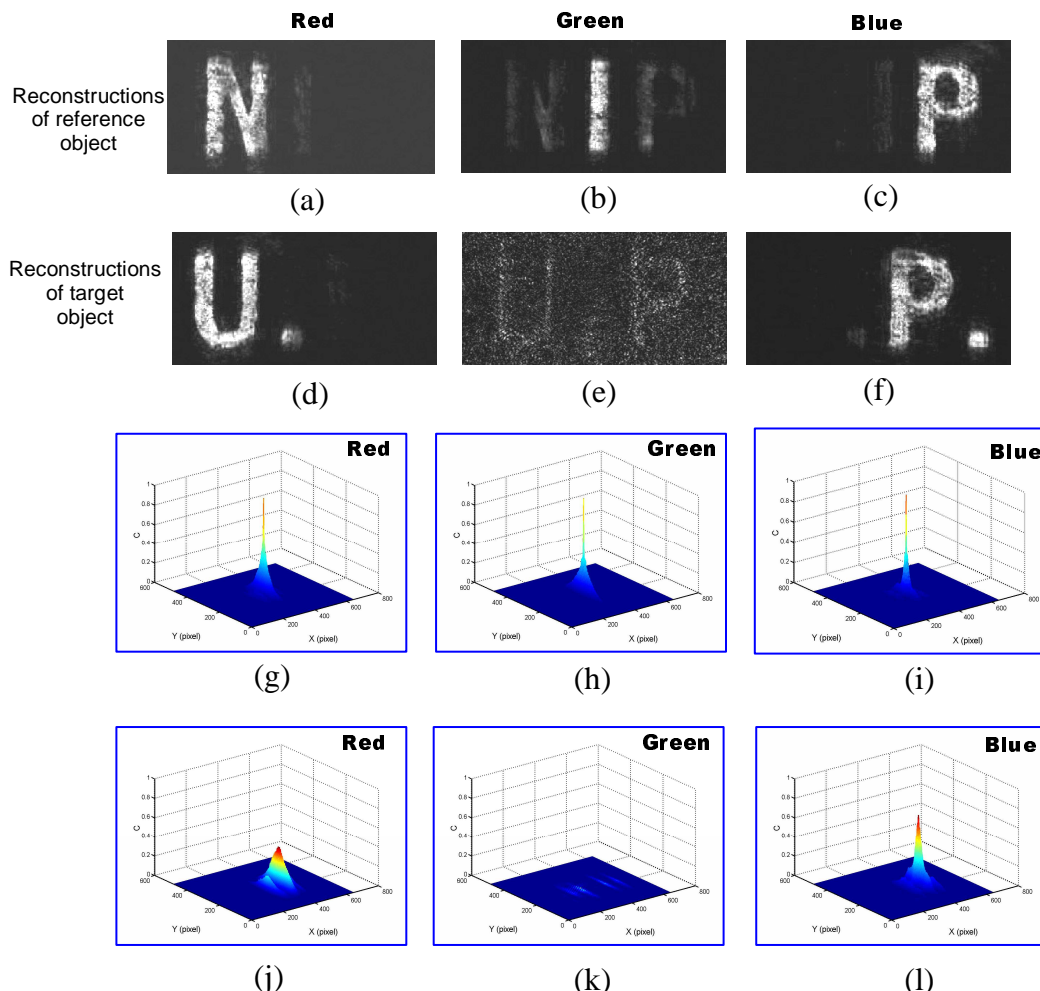


Fig. 3. Colored object recognition. First row (top): (a) R, (b) G, and (c) B reconstructions of reference object. Second row: (d) R, (e) G and (f) B reconstructions of target object. Third row: Autocorrelations of R (g), G (h) and B (i) reconstructions. Fourth row: (j), (k) and (l) are cross-correlations of R (j,  $C_{\max}=0.42$ ), G (k,  $C_{\max}=0$ ) and B (l,  $C_{\max}=0.72$ ) reconstructions of the reference and target.

### Summary and conclusions

We have demonstrated colored object recognition by full-color digital holography using an optically-pumped  $H_2$  Raman shifter. Pumping with an elliptically polarized beam, increases the number of intense, polarized and coherent lines from the shifter. Seventeen wavelengths were detected at a pump wavelength of 532 nm and gas pressure of 0.69 MPa. We have employed the convolution method to obtain scale-invariant hologram reconstructions at different wavelengths. Colored object recognition was implemented accurately using the RGB Raman output lines and multi-channel correlation of hologram reconstructions. Our results provide the groundwork for the use of full color digital holography in spectral imaging using the Raman shifter as light source.

### Acknowledgments

PCASTRD-DOST and OVCRD-University of the Philippines Diliman for research grants.